SANDIA REPORT
SAND2009-5995
Unlimited Release
Printed September 2009

Advanced Optical Measurements for Characterizing Photophysical Properties of Single Nanoparticles

Ryan W. Davis, Dulce C. Arango, David R. Wheeler, Ronen Polsky, Susan M. Brozik

Prepared by
Sandia National Laboratories
Albuquerque, New Mexico 87185 and Livermore, California 94550

Sandia is a multiprogram laboratory operated by Sandia Corporation,
a Lockheed Martin Company, for the United States Department of Energy's
National Nuclear Security Administration under Contract DE-AC04-94AL85000.

Issued by Sandia National Laboratories, operated for the United States Department of Energy by Sandia Corporation.

Available to DOE and DOE contractors from
U.S. Department of Energy
Office of Scientific and Technical Information
P.O. Box 62
Oak Ridge, TN 37831

Telephone: (865)576-8401
Facsimile: (865)576-5728
E-Mail: reports@adonis.osti.gov
Online ordering: http://www.osti.gov/bridge

Available to the public from
U.S. Department of Commerce
National Technical Information Service
5285 Port Royal Rd
Springfield, VA 22161

Telephone: (800)553-6847
Facsimile: (703)605-6900
E-Mail: orders@ntis.fedworld.gov
Online order: http://www.ntis.gov/help/ordermethods.asp?loc=7-4-0#online

SAND2009-5995
Unlimited Release
Printed September 2009

Advanced Optical Measurements for Characterizing Photophysical Properties of Single Nanoparticles

Ryan W. Davis, Dulce C. Arango, David R. Wheeler, Ronen Polsky, Susan M. Brozik

Biosensor and Nanomaterials Department
Sandia National Laboratories
PO Box 5800
Albuquerque, NM 87185-1425

Abstract

Formation of complex nanomaterials would ideally involve single-pot reaction conditions with one reactive site per nanoparticle, resulting in a high yield of incrementally modified or oriented structures. Many studies in nanoparticle functionalization have sought to generate highly uniform nanoparticles with tailorable surface chemistry necessary to produce such conjugates, with limited success. In order to overcome these limitations, we have modified commercially available nanoparticles with multiple potential reaction sites for conjugation with single ssDNAs, proteins, and small unilamellar vesicles. These approaches combined heterobifunctional and biochemical template chemistries with single molecule optical methods for improved control of nanomaterial functionalization. Several interesting analytical results have been achieved by leveraging techniques unique to SNL, and provide multiple paths for future improvements for multiplex nanoparticle synthesis and characterization. Hyperspectral imaging has proven especially useful for assaying substrate immobilized fluorescent particles. In dynamic environments, temporal correlation spectroscopies have been employed for tracking changes in diffusion/hydrodynamic radii, particle size distributions, and identifying mobile versus immobile sample fractions at unbounded dilution. Finally, Raman fingerprinting of biological conjugates has been enabled by resonant signal enhancement provided by intimate interactions with nanoparticles and composite nanoshells.

Contents

Introduction

Conductive and semi-conductive nanoparticles having unique electronic, catalytic or photophysical properties are considered to be promising tools applicable to nanotechnology. Even though the controlled manipulation and organization of these materials is of critical importance, there are currently few methods for generating functional and stable assemblies of bio-conjugated nanomaterials[1-3]. Numerous researchers have proposed different solutions to this challenge in order to generate structures that are both of inherent technological interest and provide a means to better understand the fundamental photophysical, chemical, and electronic properties of nanoparticles. Our approach to these ends focused on combining unique analytical methods which probe interactions at the single particle level with molecular self-assembly and recognition-based biochemical synthesis.

Several specific challenges in the realms of single molecule analysis and biochemical synthesis of nano-assemblies were addressed in this effort. These include methods for generating aggregate and single conjugate forms of nanoparticles with proteins, phospholipids, and DNA; detecting differences in the size of individual nanoparticle assemblies; temporally tracing the interaction dynamics between functionalized nanoparticle hosts and recognition targets; definining the photophysical properties of hetero-dimeric nanoparticle conjugates; specifying conditions which enable spectroscopic identification of a nanoparticle-conjugated biomolecule; and outlining potential means for deploying a functionalized nanoparticle as a multianalyte optical sensor.

Three primary single molecule optical methods, including hyperspectral fluorescence imaging (HSI), correlation spectroscopy (FCS, DLS), and surface-enhanced Raman spectroscopy were employed in this work. Together these methods enabled detection and characterization of the resulting nano-assemblies, and pave the way for next generation sensor technologies based on nanoparticle interactions with biomolecules of interest, especially genetic sequences, and peptide toxins.

Materials and Methods

1) Optical Measurements

Synthesis of heterodimeric nanoparticle conjugates

Initial experiments with nanoparticle conjugation were directed at understanding covalent and non-specific binding interactions of solution state nanoparticles. Of particular interest was the heterodimeric combination of conductive Au colloids and nanoclusters with semi-conductive core-shell CdSe fluorescent nanoparticles for assays employing resonant energy transfer (RET) or quenching as a spectroscopic indicator. Unmodified Au colloids (2 nm dia.) were purchased from Ted Pella, Inc.; amine, carboxyl, and amino-PEGylated CdSe nanoparticles (shell-core diameter = 4.5 nm) were purchased from Invitrogen, Inc.; and maleimide, amine, and streptavidin conjugated Au nanoclusters (1.4 nm dia.) were purchased from Invitrogen, Inc. For single molecule experiments described below, Au colloids or clusters were combined pairwise with either the amine or carboxyl modified CdSe nanoparticles in graded concentrations of buffered solutions (citrate, tris-HCl, PBS, and KCl) to adjust the final concentration of each analyte to 30 pM. Covalent conjugation of monoamine-modified Au colloid to carboxyl modified CdSe particles was performed by adapting the protocol of Graberek and Gergely[4]. 1 mg/ml carboxyl-modified CdSe was suspended in 0.1 M MES buffer with 0.5 M NaCl, pH 6.0 to which was sequentially added the powder form of 1-ethyl-3-[3-dimethylaminopropyl]-carbodiimide hydrochloride (EDC, final concentration = 2 mM), and following pipette stirring, the powder form of *N*-hydroxysulfosuccinimide (Sulfo-NHS, final concentration = 5 mM). Following 15 minutes of reaction time, the solution was transferred to a buffer activated 100kD cutoff centrifugation column for separation of the coupling reagents from the CdSe nanoparticles. After centrifugation at 4000 rpm for 5 minutes or until ~90% of the solution had passed through the centrifugation column, monoamine-modified Au colloid in buffer (final concentration of 1:1 mol/mol Au:CdSe) was added to the centrifugation column, agitated gently, and stored for 2 hours at room temperature. The final Au-CdSe heterodimeric conjugates were then washed in a centrifuge tube as performed above, and suspended in 10 mM PBS for spectroscopic studies.

Synthesis of nanoparticle-DNA conjugates

For investigations involving nanoparticle-DNA conjugates for hybridization sensing, coupling methods similar to those employed for synthesizing nanoparticle heterodimers were adopted. Non-self hybridizing ssDNA and the appropriate complement sequences were purchased from IDT, Inc. in 21mer and 30mer lengths. In specified samples, sequences were further modified by the provider to introduce a 5'-amine for EDC conjugation with carboxyl-conjugated nanoparticles as well as a 5'-thiol, 3'-Cy3 fluorescently labeled ssDNA for assessing degree of conjugation and quenching.

Coupling of the 5'-amino-ssDNA with carboxyl-modified CdSe was performed by adapting the EDC synthesis described above. 1 mg/ml EDC and Sulfo-NHS were dissolved in separate vials of 2x PBS, pH 6 solution. Once the reagents had dissolved, four times molar excess of EDC was then added to 20 nmoles of carboxyl-modified CdSe in 1 ml of the PBS. Immediately following, Sulfo-NHS was added to the solution at 8 times molar excess, and allowed to react for 15 minutes. The solution was then transferred to a buffer activated 100 kD cutoff centrifugation column for separation of the coupling reagents from the carboxyl-modified CdSe nanoparticles. After centrifugation at 4000 rpm for 5 minutes or until ~90% of the solution had passed through the centrifugation column, ssDNA in PBS (final concentration of 10:1 mol/mol amino-DNA:CdSe) was added to the centrifugation column, agitated gently, and stored for 2 hours at room temperature. The final ssDNA-CdSe conjugates were then washed in a centrifuge tube as performed above, and suspended in PBS. Prior to spectroscopic imaging studies, serial dilution was employed to dilute the conjugates to 100 pM, and these were combined with similarly coupled complement ssDNA for hybridization studies.

1-to-1 ssDNA-Au nanocluster conjugates were performed by reacting monomaleimide modified Au nanoparticles with 5'-thiol ssDNA. The modified Au nanoclusters were dissolved in 20 µL of DMSO, and diluted 10x in water. Aliquots of this solution were then transferred to thiolated ssDNA solutions at a rate of 10x molar excess and the reaction was incubated for 18 hours at 4°C. Unreacted Au clusters were then separated

from the ssDNA-nanoparticle conjugates in 100 kD cutoff centrifugation columns by spinning at 4000 rpm for 5 minutes. PBS buffer was added back to the columns to 0.5 ml, and the preparations transferred to Eppendorf tubes for spectroscopic analysis.

In order to define conditions under which ssDNA could be coupled in a 1-to-1 fashion with a surface modified fluorescent nanoparticle, a different coupling chemistry was adopted[5]. In this case, amino-PEGylated CdSe was dissolved in 1x PBS, pH 7.2 containing 1 mM EDTA for a final nanoparticle concentration of 8 μM. Sulfosuccinimidyl-4-(*N*-maleimidomethyl)cyclohexane-1-carboxylate (SMCC) was dissolved in the same buffer, and 4 different volumes corresponding to a logarithmic range of concentrations between 1x molar excess and 75x molar excess (in addition to a SMCC-free control) were pipetted into the amino-PEGylated CdSe nanoparticle suspension. After gentle agitation for one hour at 4°C, the solutions were transferred to 100kD cutoff centrifugation columns, and centrifuged for 30 minutes at 1000 x g. The nanoparticles were then recovered by adding buffer to the columns up to 0.5 mL. 5'-thio, 3'-Cy3 ssDNA was then dissolved in 1x PBS, pH 7.2 containing 1 mM EDTA, and combined with the SMCC activated amino-PEGylated CdSe nanoparticles at equimolar ratio. The reaction tubes were wrapped in foil and gently agitated for 2 hours at 4°C. The solutions were then removed from the reaction tubes and transferred to 100 kD cutoff centrifugation columns which were spun at 1000 x g for 30 minutes. Finally, the contents which passed through the column were subjected to fluorescence analysis to ascertain the degree of labeling.

Synthesis of Au nanoparticle-GroEL conjugates

Electrostatic binding of GroEL to 1.4 nm Au nanoclusters and 2 nm Au colloid was attempted by incubating GroEL at 60°C for 10 minutes with the following reagents: 100 mM potassium chloride, 25 mM tris-hcl, 25 mM magnesium chloride, 36 μM adenosine-5'-triphosphate. After 10 min incubation, ATP triggered GroEL was incubated with 3 x 10^{12} gold colloids and nutated for 1 hour at room temperature. The GroEL and gold nanoparticle complex was run through a 100,000 MWCO Centricon centrifugal filter (Millipore, Brillerica, MA) for 3 min at 4000 rpm and washed twice with 500 μL of water

for 5 minutes and 4000 rpm before being brought to a final volume of 200 µL with water. Final protein concentrations were determined using absorbance at 280 nm and extinction coefficients of 23, 800 M^{-1} cm^{-1}.

Au nanoclusters were directly conjugated to GroEL by adapting the method of Hashida, et. al[6]. Five times molar excess of dithiothreitol (DTT) was added to 200 µL of a 10 mM tris-HCl, pH 7.5 buffered solution of 10 µM GroEL. This solution was incubated at room temperature for one hour, after which the DTT was removed in a BIO-Spin 30 Tris centrifugation column by spinning at 4000 rpm for 3 minutes. Monomaleimide Au cluster was dissolved in 1:10 ratio of DMSO:water and 7.5 times molar excess was then added to the protein solution for a total volume of 400 µL. The resulting nanoparticle – protein solution was incubated for 18 hours at 4°C, after which, the conjugate was separated from the unbound nanoparticles in a BIO-Spin 30 Tris centrifugation column as described above, and stored at 4°C.

Self assembly of Au nanoparticle-SUV assemblies

Self assembly of small unilamellar vesicles (SUVs) was initiated by combining 1,2-dipalmitoyl-sn-glycero-3-phosphocholine (DPPC) and 1,2-dipalmitoyl-sn-glycero-3-phosphothiethanol (DPPTE) (Avanti Polar Lipids, Inc.) as chloroform solutions to a round bottom flask. The chloroform was then removed by streaming dry N_2 until a lipid film was apparent, followed by placing the preparation under vacuum for 1 hour. Once the solvent had been removed 100 mM PBS, pH 7.2, was added to adjust the final phospholipid concentration to 1.5 mg/ml. Molar ratios of POPC:DPPTE corresponding to 1:10, 1:50, and 1:100 were investigated for Au nanocluster binding. The resulting liposome suspension was then subjected to ultrasonication using a Branson 250 Ultrasonicator (microtip setting = 6, duty cycle = 20 %) for 10 min. at 4º C, thus generating small (<100 nm dia.) unilamellar vesicles.

Monomaleimide Au nanoclusters were dissolved in 20 µL of DMSO, and diluted 10x in water. Aliquots of this solution were then transferred to the SUV suspensions at a rate of 5x the molar equivalent of the DPPTE component and the reaction was incubated for 18

hours at 4°C. Unreacted Au clusters were then separated from the SUV-nanoparticle conjugates in centrifugation columns by spinning at 4000 rpm for 5 minutes. PBS buffer was added added back to the columns to 0.5 ml, and the preparations transferred to Eppendorf tubes for spectroscopic analysis or silver enhancement.

Deposition of Silver thin films on Au nanoparticle conjugates

The LI Silver Enhancement (LIS) kit provided by Invitrogen, Inc. was used to generate thin films of Ag onto Au nanoclusters which had previously been conjugated to a protein or phospholipids in SUVs. Samples to be coated with silver were first desalted in a water activated 100 kD cutoff centrifugation column at 4000 rpm for 5 minutes, or until ~90% of the solution had passed through the column. Subsequent steps were performed in the dark, without removing the solution from the centrifugation tube. Immediately after combining the LIS enhancer and developer reagents 0.5 ml was added, with pipette stirring, to centrifugation columns containing the protein- or SUV-conjugates of interest. In order to control the thickness of the silver layer, centrifugation was initiated at time points corresponding to 0, 5, and 10 min following exposure to the enhancer/developer cocktail using the column, speed, and time specifications described above. After centrifugation was complete, 0.5 mL of buffer solution was added to the centrifugation columns, and the preparations transferred to a light-protected Eppendorf tube for spectroscopic analysis.

Hyperspectral Confocal Fluorescence Imaging

Spectral image data were collected using a scanning confocal hyperspectral microscope described by Sinclair et. al[7]. In this system, fluorescence emission is excited by a continuous wave 488 nm sapphire laser and collected at each point over a spectral range of 500 nm to 800 nm using a prism-based EMCCD spectrometer. Vertical binning of the spectral data in 512 EMCCD pixels combined with a push- broom readout mode[8] allows data collection to be performed at a maximum sustained readout rate of 8.3 Mbits/s at a spectral resolution >3 nm. In the described experiments, low resolution imaging was performed using an infinity corrected 20x objective (Nikon, PlanApo NA = 0.75), corresponding to an in-plane voxel dimension of 0.24 μm per side. High resolution

imaging was performed using an infinity corrected 60x oil-immersion objective (Nikon, PlanApo VC NA = 1.40), corresponding to an in-plane voxel dimension of 0.12 μm per side. In both cases, 204 x 204 point spectral arrays were collected at a scan rate of 4167 spectra per second, for an overall single image collection time of ~10 sec. For evaluation of the time dependent effects, images were collected at pre-programmed delay intervals at arbitrary spatial locations on the sample.

Fluorescence Correlation Spectroscopy

High temporal resolution photon counting data were collected using a custom dual channel confocal system. This system excites fluorescence using a spatially filtered continuous wave 488 nm Ar ion laser, allowing complimentary experiments excitation between this system and the confocal fluorescence hyperspectral imager. Fluorescence emission from emitting species in the confocal volume is collected using an infinity corrected 20x objective (Nikon, PlanApo NA = 0.75), corresponding to an in-plane single voxel volume of ~1 fL. Output from two fiber coupled avalanche photodiode detectors (APD, EG&G, Inc) is received at a multi-channel couter-timer device (National Instrument, Inc.) allowing high efficiency sustained single photon detection at a maximum rate of 40 MHz. Spectral windows are defined by orthogonal filter sets (500-525 nm, 535-550 nm, 575-650 nm; Chroma, Inc) for spectral cross-correlation, and identical filters for high-accuracy cross-correlation at short correlation times. Calibration of the confocal volume is performed preceding each measurement using standard solutions of 525 nm-emitting fluorescent nanoparticles at concentrations of 100 pM and 1 nM. A custom C/C++ interface allows temporal binning of counted photons, histogramming of photon arrival periods, rejection of after-pulse events, and temporal auto- and cross-correlation of spectral channels, each at arbitrary (signal dependent) temporal scales. Following calculation of correlation functions, several diffusion models with user-defined constraints are available, and are implemented through a Levenberg-Marquardt (LM) non-linear least squares fitting algorithm.

Photon Correlation Spectroscopy/Dynamic Light Scattering

Photon correlation spectroscopy (PCS, also known as DLS) has been implemented as a second capability using the same hardware and software as the photon counting aparatus described in the fluorescence correlation spectroscopy method. In this system, a spatially filtered continuous wave 488 nm Ar ion laser is split with a cube beam splitter, providing two equal length optical arms for cross-correlation analysis. The experimental arm contains a cuvette with the aqueous nano-assembly sample of interest, whereas the reference arm contains a matched cuvette with either ultra-pure water or the sample buffer. Scattered light from each arm is collected normal to the direction of propagation of the laser and focused into the respective APD fiber pinhole. Following software cross-correlation of the reference and experimental scatter, analysis is performed using a three parameter sum of exponentials and variance calculated using a second-order cumulant model, using LM non-linear least squares fitting, as above.

Raman Spectroscopy

Raman spectroscopy was performed on evaporation deposited and solution phase nanoparticle assemblies using a Nicolet Almega Raman confocal microscope system (Thermo Scientific, Inc.) using a 40x objective lens (0.9 NA, Olympus, Inc.). Excitation of plasmon resonance in conductive nanomaterial composites and Raman scattering was performed using a 532 nm Nd-YAG laser with illumination power of 10 mW at the sample, measured with a pre-calibrated Si photodiode power sensor (Thorlabs, Inc.). Spectra were acquired using a1200 line/mm gratings with a spectral range of 400 cm^{-1} – 2800 cm^{-1}, and a spectrograph aperture of 50 mm. Typically spectra were integrated over 30 seconds, with averaging from 2 independent measurements. In some cases, however, time series were collected without averaging, with integration times of 2 seconds per spectrum.

2) Electrochemical Measurements

Preparation of GroEl and gold nanoparticle complex

Chaperonin 60 (GroEL) was purchased from Sigma (St. Louis, MO). Magnesium chloride, potassium chloride, tris-hcl and adenosine-5'-triphosphate (ATP) were

purchased from Sigma (St. Louis, MO). All solutions were prepared with 18 MΩ water using a Barnstead Nanopure water purifier (Boston, MA). 2nm colloidal gold was purchased from Ted Pella, Inc (Redding, CA).

GroEL (1.25 μM) was incubated at 60°C for 10 minutes with the following reagents: 100mM potassium chloride, 25 mM tris-hcl, 25 mM magnesium chloride, 36 μM adenosine-5'-triphosphate. After 10 min incubation, ATP triggered GroEL was incubated with 3 x 10^{12} gold colloids and nutated for 1 hour at room temperature. The GroEL and gold nanoparticle complex was run through a 100,000 MWCO Centricon centrifugal filter (Millipore, Brillerica, MA) for 3 min at 4000 rpm and washed twice with 500 μL of water for 5 minutes and 4000 rpm before being brought to a final volume of 200 μL with water. Final protein concentrations were determined using absorbance at 280 nm and extinction coefficients of 23, 800 M^{-1} cm^{-1}.

Release of gold nanoparticles

After incorporating gold nanoparticle into GroEL and immobilization of GroEL, the release of gold was induced by the addition of ATP. The immobilized GroEL and gold nanoparticle complex was incubated at 70° C for 10 minutes in the same buffer used for incorporation of gold nanoparticle. The ATP induces a conformational change which evidently releases the gold nanoparticles from the GroEL pore.

Preparation of diazonium functionalized chaperonins immobilized onto carbon electrodes

Chaperonin 60 (GroEL) was purchased from Sigma (St. Louis, MO). Sodium phosphate monobasic, sodium phosphate dibasic, sodium carbonate, sodium bicarbonate, and 30% H_2O_2 were purchased from Sigma (St. Louis, MO). Fluoroboric acid was purchased from Sigma-Aldrich. 1-Ethyl-3-[3-dimethylaminopropyl]carbodiimide hydrochloride (EDC), 4-aminobenzoic acid and N-hydroxysuccinimide (NHS) were purchased from Acros Organics (Beel, Belgium). All solutions were prepared with 18 MΩ water using a Barnstead Nanopure water purifier (Boston, MA). All electrochemical measurements were performed on a PGZ 100 Voltalab potentiostat (Radiometer Analytical, Lyon,

France) and were measured versus an Ag/AgCl reference and Pt counter electrode (Bioanalytical Systems, West Lafayette, IN). The Ag/AgCl reference electrode was calibrated versus iron (III) chloride and ferricyanide and was found to be within ±1-3 mV of published formal potentials. 3 mm glassy carbon electrodes (GCE) were polished by 1, 0.3, and 0.05 μm alumina slurry (Buehler, Lake Bluff, IL) on a polishing pad with sonication in ethanol and water in between steps.

Preparation of Carboxyl Diazonium Molecule

4-aminobenzoic acid (2.74 g, 20.0 mmol) was dissolved in fluoroboric acid (48%, 14.6 g, 80 mmol) and water (20 mL). The solution was heated until the aniline completely dissolved then cooled in an ice water bath. Sodium nitrite (1.46 g, 21.2 mmol) dissolved in water (4 mL) was added drop wise while the reaction mixture stirred. The solution was allowed to warm to room temperature and concentrated via rotary evaporation to half the original volume. The solution was cooled in an ice bath, the white solid was collected and washed with cold ether to give 1.24 g (26%) of the desired diazonium salt.

Diazonium GroEL modification and protein deposition

3 mg of carboxyl diazonium, 19 mg EDC, and 11.5 mg NHS were mixed in 1 ml of water for 10 minutes. 10μLs of this solution was added to 200 μLs of 5 mg/ml GroEL for 2 hours. The solution was then run through a 100,000 MWCO Centricon centrifugal filter (Millipore, Billerica, MA) for 3 min at 4000 rpm and washed twice with 200 μL water for 5 min and spun at 4000 rpm before being brought to a final volume of 200 μL with water. Final protein concentrations were determined using absorbance at 280 nm and extinction coefficients of 23, 800 M-1 cm-1.

A 20 μL drop of 2 mg/ml GroEL solution was placed onto the working area of a GCE in connection to an Ag/AgCl reference and Pt wire counter electrode respectively. A cyclic voltammogram was run from 0 to -1000 mV for 5 cycles at 100 mV/sec. The electrodes were then washed with water and dried under a stream of argon.

Immobilization of GroEL and gold nanoparticle complex on thiolated surfaces

1,8-ocatanedithiol was purchased from Fluka. Gold electrodes were made in house. Solutions were prepared with 18 MΩ water using a Barnstead Nanopure water purifier (Boston, MA). Self-assembled thiolated monolayers were prepared by immersing the gold substrate in millimolar ethanolic solution of thiols for 12-16 h. The ethanolic solution was bubbled with nitrogen and kept under nitrogen atmosphere in the dark during the immersion. After the modification, the samples were removed from the ethanolic solution, rinsed with ethanol and Nanopure water and then blown dry with nitrogen. A 15 μL aliquot of 2 mg/ml GroEL and gold nanoparticle complex solution was aliquoted onto thiolated gold surfaces and incubated overnight at room temperature. After overnight incubation, the samples were removed from the GroEL and gold nanoparticle solution, rinsed with Nanopure water and then blown dry with nitrogen.

Mutagenesis of GroEL D490C

One of the strategies to immobilize a functional GroEL was to genetically modify the GroEL protein to facilitate immobilization. Following published protocol[9] Asp490, which is located on the outer surface of the equatorial domain[10], was substituted with cysteine for direct labeling with biotin maleimide.

Overexpression and purification of GroEL D490C

A gene encoding GroEL, derived from reported sequences of the protein and found naturally in *E. coli,* was chemically synthesized by Integrated DNA Technologies, Inc. This GroEL gene was designed with specific restriction sites that facilitated the cloning process. In addition sequences were modified for successful intra-cellular expression. The sequence for GroEL is shown below.

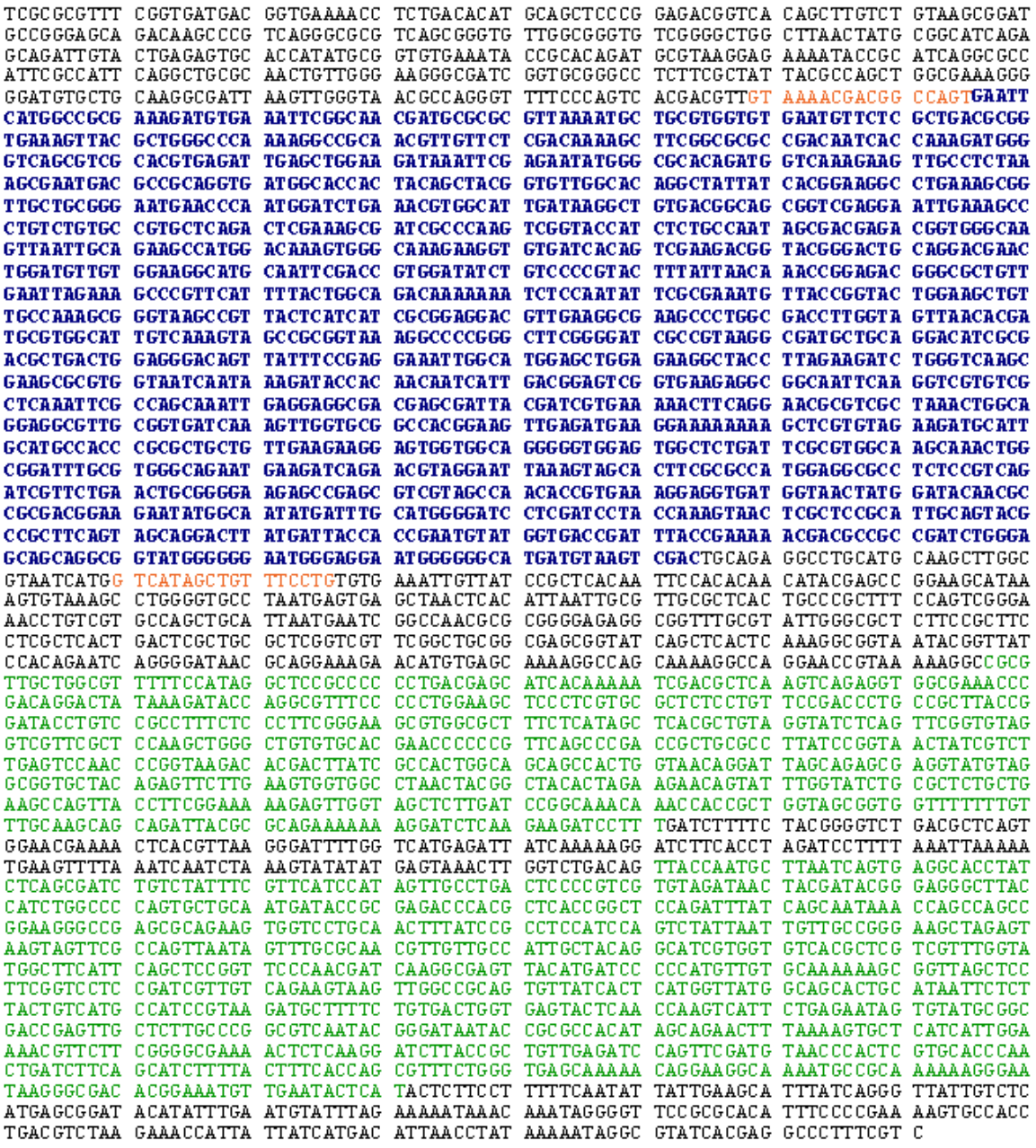

…Genetic sequence produced by Integrated DNA Technologies based on the sequence of the protein produced in *E. coli*….

We cloned the genetic sequence into the expression vector pET21c which was purchased from Novagen (Madison, WI). Restriction enzymes, BL21 cells, calf intestinal alkaline phosphatase, and ligation kit utilized for cloning the GroEL gene into the vector was purchased from New England Biolabs (Ipswich, MA).

Rhodanese was purchased from Sigma (St. Louis, MO). Sephacryl HR-300 was purchased from Sigma Aldrich. DE-52 anion-exchange resin was obtained from GE Healthcare (Clifton, NJ). The GroEL Monoclonal Antibody (9A1/2) was purchased from Assay Designs (Ann Arbor, MI).

Construction of GroEL expression plasmid pET-D490C

GroEL expression plasmid pET-D490C was constructed by inserting a 1.7-kilobase EcoRI-SalI fragment including the GroEL gene isolated from pUC57 vector (vector from Integrated DNA Technologies) into pET21c at EcoRI-SalI treated with calf intestinal alkaline phosphatase. This new vector was transformed into *E. coli* BL21 cells (New England Biolabs) for protein expression. The transformed cells were plated on LB plus ampicillin plates and individual colonies picked for screening and analysis.

Expression of GroEL in pET21c vector

GroEL recombinant plasmid was grown in 50 mL of LB medium containing ampicillin (50 μg/mL) at 37ºC, shaken at 200 rpm, and grown overnight. The following morning, 1L of LB media with 50 μg/ml of ampicillin was pre-equilibrated to 37ºC and then inoculated with 5mLs of fresh overnight culture. The optical density at 600 nm was measured every 30 min and when the cells reached an optical density of 0.4, 1mM IPTG (final concentration) was added to the culture. The cultures were further grown until the cells reached an optical density of 2.0. Cells were collected by centrifugation at 4500*g* for 5 minutes and washed with 50 mM sodium phosphate buffer, pH 7.0. 3 grams of cell paste from induced cell culture was suspended in buffer 1 (50mM tris-HCl, pH 8.0, 1mM EDTA, 1mM DTT, and 0.1 mM PMSF). In addition, 3mL of 10 mg/mL of lysozyme was added to the induced culture. The cells were nutated in buffer 1 for 5 minutes before sonication. Sonication was carried out for 2.5 minutes on ice. Cell lysate was then centrifuged at 100,000*g* for 1 hour in an ultracentrifuge. At this point the supernatant solution contained the soluble protein and was ready for further purification.

Purification of GroEL

The supernatant containing the GroEL protein was treated with 25 mL packed volume of DE-52 anion exchanger equilibrated to pH 8.0. The resin and supernatant was mixed for 30 min on a nutator and centrifuged at 3000*g* for 15 minutes. GroEL in the supernatant solution was precipitated with ammonium sulfate (50% saturation) and equilibrated for 1 h, and the precipitate was collected by centrifugation at 12,000 *g* for 30 min. The ammonium sulfate precipitate was dissolved in 2 mL of buffer 1 and GroEL was purified by gel filtration chromatography on Sephacryl HR-300 column equilibrated with buffer 1. The concentration of GroEL was determined using absorbance at 280 nm and extinction coefficients of 23,800 M^{-1} cm^{-1} [11]. Purified GroEL was dialyzed against 50 mM tris-HCl, pH 7.5, and 1 mM DTT. GroEL aliquots were frozen in liquid nitrogen and stored at -80ºC.

Folding Assay

The folding activity of GroEL was tested by detecting the denaturation and renaturation of rhodanese as described by Mendoza *et al* [12]. Rhodanese activity was detected based on the method of Sorbo[13] as described in[11].

Results

1) Optical Measurements

Bulk characterization of nanoparticle-DNA conjugates

Few traditional bulk analytical techniques are available for probing detailed nanoscale architechture; however, where possible, UV-Vis absorption was employed to address degree of labeling in DNA-nanoparticle and protein-nanoparticle conjugation.

To assess the effect of different molar excess treatments of the SMCC reagent on coupling of ssDNA to amino-PEGylated CdSe nanoparticles, the fluorescence intensity (530 nm ex., 565 nm em.) of the flow-through of 5'-thio, 3'-Cy3-ssDNA was measured for different SMCC ratios to the nanoparticle and DNA. The results of this assay are depicted in Figure 1.

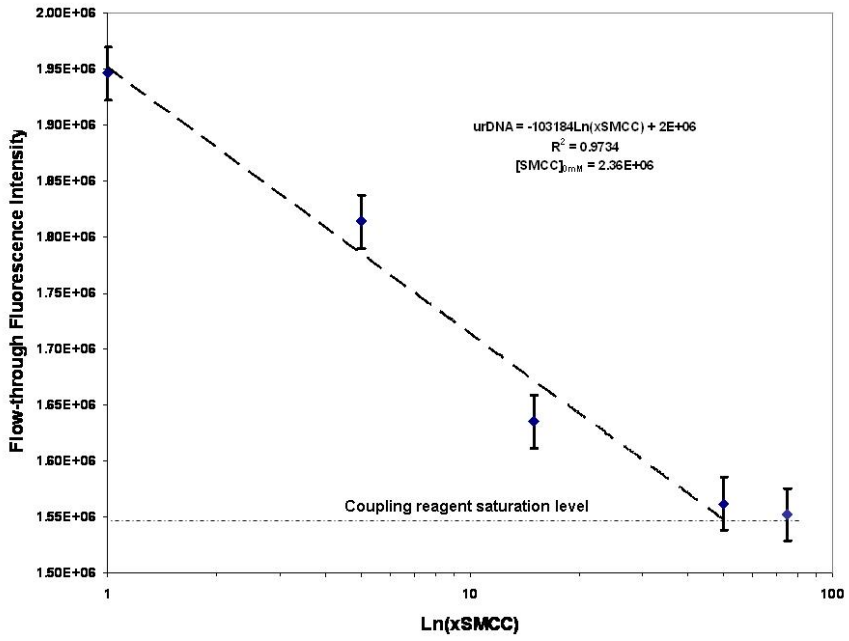

Fig. 1: SMCC flow-through fluorescence intensity. Saturation of the coupling reagent at 1:1 ssDNA:CdSe is achieved at molar excess >50.

The maximum yield of this assay was calculated based on the difference between the 0 mM SMCC and the 50x molar excess SMCC, and was found to be ~10%. Although this yield is unsatisfactory for most single molecule assays, the result allowed the determination that 10x excess of 5'-thio, 3'-ssDNA is necessary for generating a high yield of 1:1 ssDNA-CdSe nanoparticle conjugates under conditions of saturating SMCC. The linear fit to the single logarithmic plot yields an exponential increase of single conjugates with increasing SMCC, indicating a single-step activation mechanism of 20 and 30mer thiolated ssDNA.

Hyperspectral imaging of fluorescence from nanoparticle conjugates

Initial studies were performed on CdSe nanoparticles at various buffer strengths and concentrations to determine conditions necessary for single particle hyperspectral fluorescence imaging experiments. It was found that evaporative deposition of polymer stabilized CdSe particles are insensitive to the osmotic strength of the buffer solution at concentrations below ~100 pM, producing diffraction limited emission from individual

particles with signal-to-noise ratio >4:1. Furthermore, high intensity aggregates were observed in <1% of depositied particles. An example of hyperspectral fluorescence data obtained in this manner is shown in Figure 2.

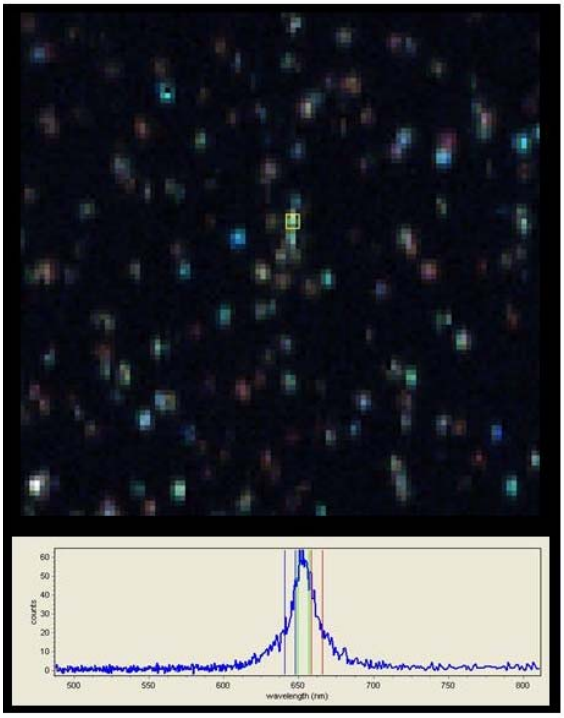

Fig. 2: Hyperspectral fluorescence image of individual CdSe nanoparticles immobilized on a coverslip by evaporation from a 30 pM solution. False color spectra windows are indicated in the spectrum at the bottom of the image, with the spectrum of a single (aggregate) region designated by the yellow box near the center of the image.

In addition to demonstrating high signal-to-noise single particle fluorescence imaging of CdSe nanoparticles, the data are suggestive of intra-batch deviation from a single nanoparticle preparation. The false color image highlights this deviation by clearly demarking individual particles which exhibit shifts >5 nm from the ideal emission at 655 ± 5 nm, FWHM, as well as multi-particle aggregates which are colored white. Previous studies on the photophysical properties of CdSe core-shell nanoparticles[14], and fluorescent nanoparticles in general[15], suggest that the spectral properties observed are indicative of differences in the size, core-shell compositions, and crystal lattice properties of the individual particles.

Assessment of the photophysical interactions between amino-PEGlyated CdSe and Au nanoparticles was performed by adsorption of individual and covalent nanoparticle conjugates in solution in an imaging cell. Data was collected in the form of single particle fluorescence emission spectra under continuous laser exposure for 18 scans (250 sec), to observe potential photodegredation or RET effects between the nanoparticle conjugates. A trace of the average temporal intensity of isolated amino-PEGylated CdSe (N=81) and covalent conjugates of the same with Au-colloids (N=74) is depicted in Figure 3.

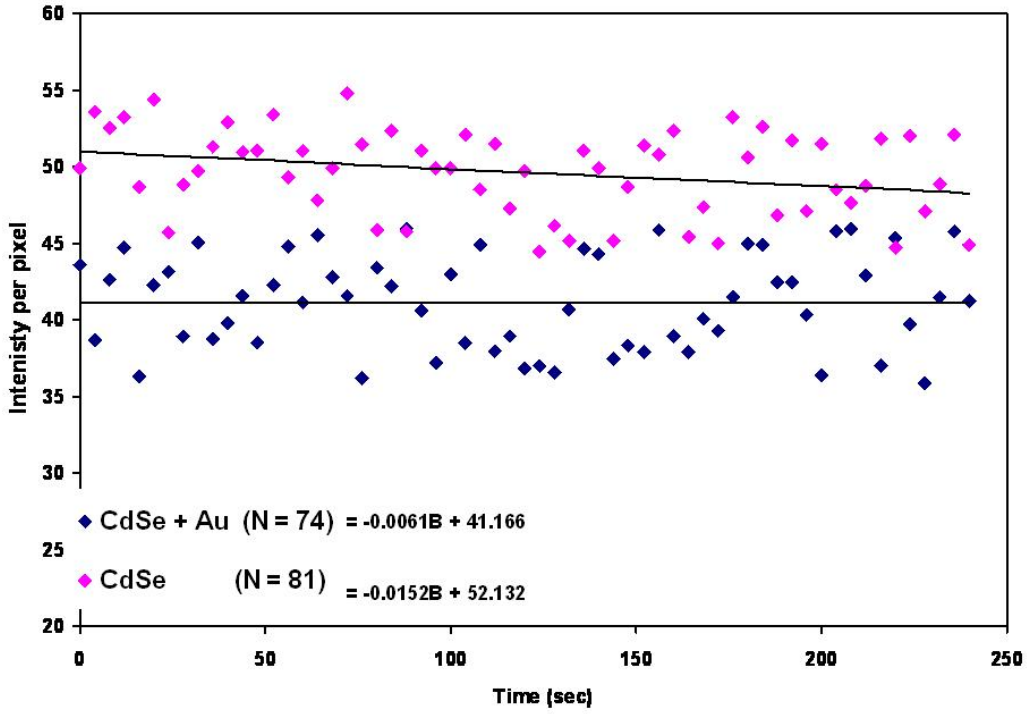

Fig. 3: Temporal evolution of fluorescence from single CdSe nanoparticles and CdSe-Au colloid conjugates over 18 image scans. Linear fits to the experimental data are depicted in the low left corner of the image.

1-to-1 covalent conjugation of amino-PEGylated CdSe to Au colloid replicates the closest possible spatial interaction of this pair of nanoparticles (~ 4.5 nm, surface to surface), revealing the expected range for potential resonant energy transfer (RET) effects. Spectral fluorescence imaging of conjugated and unconjugated CdSe - Au pairs

revealed a 20.1% decrease in emission intensity in the conjugated case, corresponding to a RET quenching of emission from CdSe to the plasmon absorbance of the Au nanoparticle. Assuming a Förster – type process (r^6 dependence on separation, with isotropic alignment of spherical emission dipole), the quenching efficiency corresponds to a calculated RET radius of 6.9 nm. This result is within the instrumental resolution to allow the detection of non-specific Au-CdSe interactions, thus allowing this sub-population of conjugates to be separated from recognition-based binding events incorporating compliment ssDNAs. An additional observation from this experiment includes decay of the fluorescence emission intensity with exposure time, indicating the possibility of photo-degredation of the polymeric shell enveloping the CdSe particle, potentially from generation of reactive oxygen species in the deposition buffer. In similar experiments, dramatic fading of the CdSe emission over a similar time scale was observed, and attributed to wicking of acetone from the coverslip-sealing, allowing solvent into the sample volume.

Following successful conjugation of ssDNA to CdSe and Au nanoparticles, initial DNA hybridization studies were performed as depicted in Figure 4. In these experiments, hyperspectral imaging was employed to observe the interaction of fluorescent DNA labels (distally conjugated to CdSe) with the Au nanoparticle during DNA hybridization. This method was hypothesized to result in ~100% quenching of this fluorophore, while leaving the CdSe emission unaltered. It was determined, however, that although the signal-to-noise ratio of individual CdSe nanoparticles is sufficient for unequivocal detection, in the case of the Cy3 fluorophore, single particle detection is not feasible due to inefficient excitation by the 488 nm laser wavelength. Although this dual-label coupling scheme was desirous as a positive-control for complimentary imaging and photon counting kinetic assays of functionalized nanoparticle interactions, the inability to detect fluorescence from a single organic fluorophore under the hyperspectral confocal fluorescence imaging platform prevented further experiments using this functionalized nanomaterial.

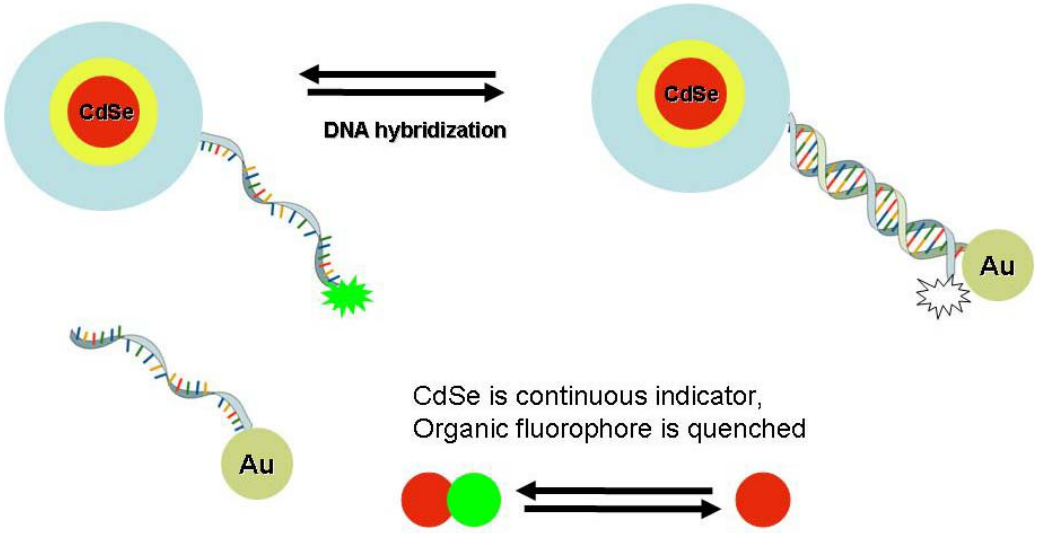

Fig. 4: Compliment ssDNA-nanoparticle conjugates for positive-controlled single molecule detection of hybridization of DNA target sequences.

Correlation measurements: interaction dynamics and particle sizing

Significant effort was leveraged to develop a unique high resolution particle sizing and reaction dynamics instrument to allow both fluorescence and elastic scattering measurements of ultra-small nanomaterial conjugates. The resulting instrument utilizes laser excitation and dual high-sensitivity APD detectors for cross-correlation analysis, thereby simultaneously providing high performance, while eliminating excitation instabilities and detector afterpulsing which contaminate fast timescale correlation data. This format also extends the concentration range for measurements by reducing the effects of multiple-scattering. A demonstration of a dynamic fluorescence correlation measurement involving a fl-biotin-streptavidin binding reaction is shown in Figure 5.

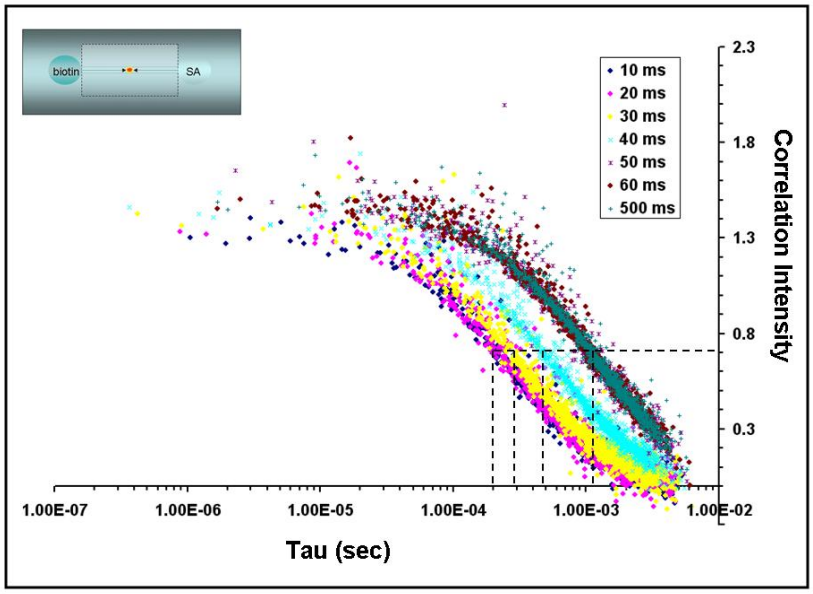

Fig. 5: Fluorescence autocorrelation time series. A schematic of the flow channel system is shown in the upper left-hand corner. Changes in diffusion of fluorescent biotin were observed at 10 msec intervals following introduction of streptavidin (SA), which reached equilibrium in ~50 ms.

Several relevant parameters of interest can be determined from the depicted fluorescence correlation decay curves. The short time-scale correlation intensity reveals the correlation volume occupation number (concentration), whereas fitting of the curves to diffusion models provides diffusion constants and thus a measure of the size of the complex and indication of shape deviations. In the biotin-streptavidin binding sytem in particular, the molecular mass of the final complex was found using the characteristic diffusion time (shown as dotted lines to the Tau axis) in the Stokes-Einstein relation, yielding ~74kD, which is consistent with previous reports for this complex.

Several measurements of functionalized nanomaterials, including sizing of protein-nanoparticle and SUV-nanoparticle conjugates, were performed using this instrument in the Photon Correlation Spectroscopy mode described above. In the case of conjugates employing Au colloids and nanoclusters, aggregation was found to be significant, and depend highly on buffer type and osmolarity. Initial Au particle sizing measurements at low osmolarity (10 mM tris-HCl) were highly inconsistent, often yielding particle sizes

of 120 nm diameter and above. Subsequent additions of KCl showed a significant size reduction, which is depicted in Figure 6.

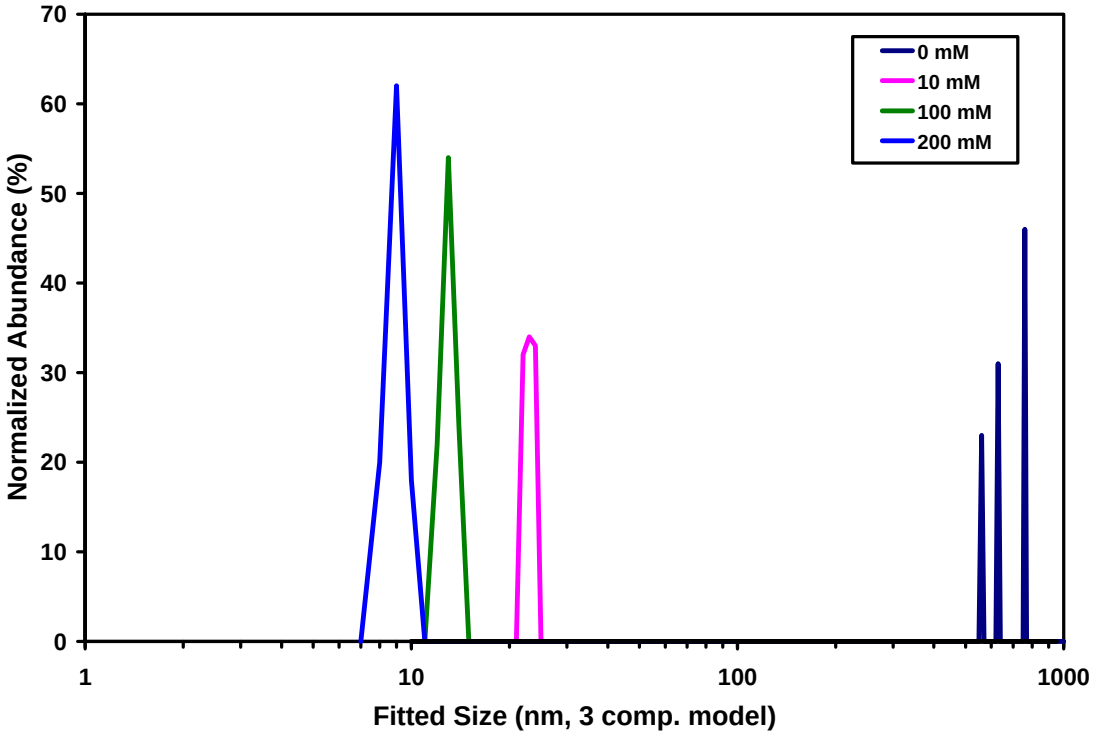

Fig. 6: The effect of osmotic strength on aggregation of gold colloids. In distilled water, Au colloid gave inconsistent results, representing a wide distribution of particles >500 nm in diameter. Increasing the osmolarity of the colloid solution with KCl showed a decrease in size and distribution of particle sizes, which was optimal at 200 mM and above.

The aggregation of Au colloid presents a difficult challenge for future efforts employing these particles in solution state chemisty which are intolerant to highly buffered solutions. Bath sonication of Au colloid samples was attempted for reducing aggregation, but negligible results were observed.

Sizing measurments of Au nanocluster-GroEL conjuates is shown in Figure 7.

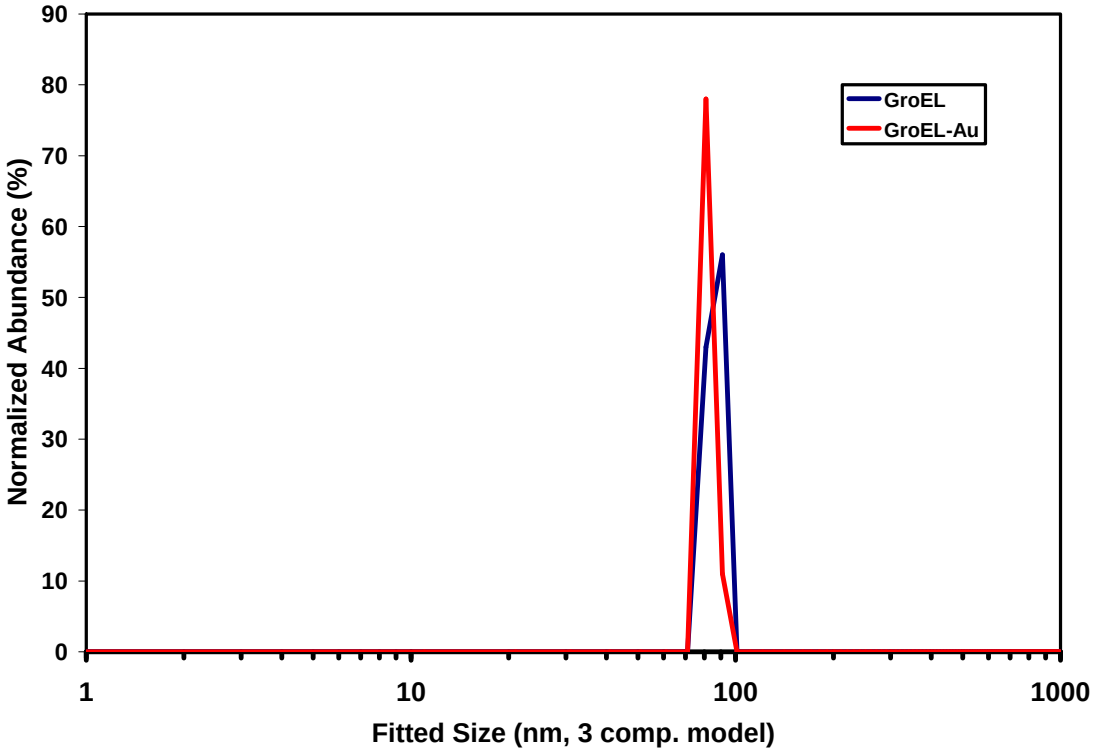

Fig. 7: GroEL and GroEL-Au conjugate size plot. The fitted particle size between the GroEL and GroEL-Au is suggestive that nanoparticle conjugation was successful; however the size of GroEL is ~10x larger than expected.

Unconjugated GroEL was found to have a particle size significantly larger than expected. Although the cause of this result is unknown, Au-GroEL conjugation appears to have been successful by the slight increase in size observed. This size increase corresponds to 1:1 conjugation based on previous sizing data collected with Au colloid alone. One possible explanation for the unexpectedly large size distribution of the protein is cross-linking of surface accessible thiol-moieties, generating polymer forms of GroEL.

Sizing measurements of SUV-Au conjugates are shown in Figure 8.

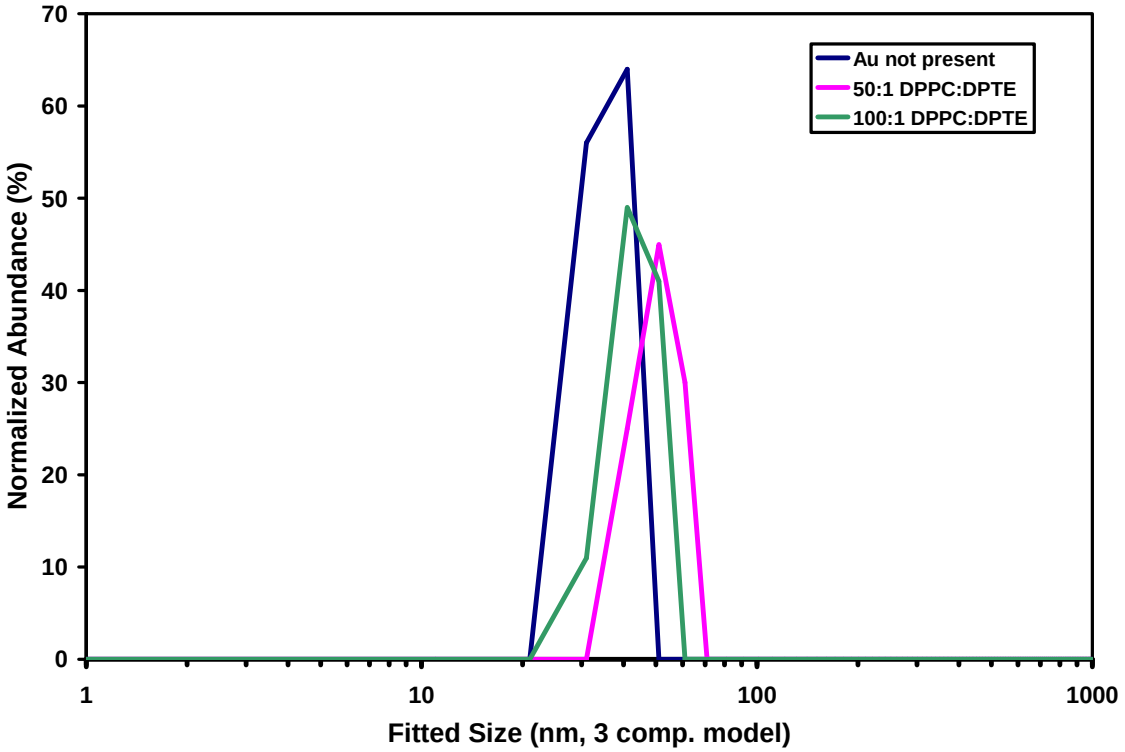

Fig. 8: Particle size distributions of DPPC:DPTE SUVs conjugated to Au nanoclusters.

DPPC:DPTE SUVs which had not been exposed to maleimide modified Au nanoclusters showed a narrow distribution of sizes centered at 33 nm dia. In preparations where the DPPC:DPTE ratio was 50:1, the distribution was slightly broader (±20 nm), and centered at 52 nm. At DPPC:DPTE ratio of 100:1, the distribution was also increased (±24), and centered around 44 nm. At DPPC:DPTE ratio of 10:1, no accurate fitting could be applied, indicative of high dispersity, and disruption of the self-assembled structure. The increases in size of the self assembled bilayer SUVs at lower DPPC:DPTE is consistent with the formation of Au-nanocluster pendants, which are intended to be used for seed formation via Ag deposition for preparation of hollow Au-Ag nanoshells.

Surface enhanced Raman spectroscopy

Raman spectroscopy is a valuable technique for uniquely identifying many chemical and biological analytes of interest. In the traditional implementation, however, pure concentrated samples are required for high quality spectra. Surface enhanced Raman spectroscopy (SERS), which couples plasmonic excitations from thin metal layers into

the vibrational modes of Raman active molecules, has been shown to amplify Raman signals $>10^{14}$, offering the possibility of generating spectra suitable for single molecule optical sensor applications[16]. In our efforts, sensing based on SERS was investigated by comparing the results of Raman signals before and after conjugation of biological molecules to Au nanoparticles, and subsequent deposition of Ag films on the resulting conjugates. Initial studies of 100 uM streptavidin solutions revealed no characteristic Raman bands following extensive integration times. Raman spectra acquired following conjugation of streptavidin to Au nanoclusters, and subsequent enhancement with different Ag layer deposition times are shown in Figure 9.

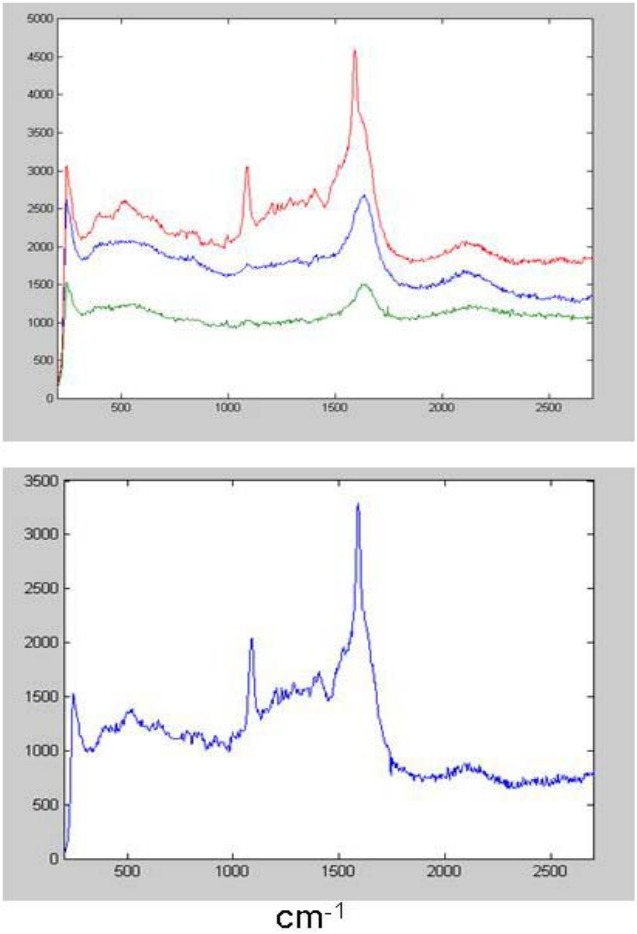

Fig. 9: Surface enhanced Raman spectra of streptavidin following conjugation to Au nanoclusters and Ag deposition. Top: raw spectra following Au-conjugation (green), 0-1 minute Ag deposition (blue), and 5 minute Ag deposition (red). Bottom: difference spectrum between 5 minute Ag deposited sample and non-deposited sample.

Spectral analysis of the resulting SERS data shows several promising characteristics from the method of Au nanoparticle conjugation and subsequent Ag deposition. Following conjugation of streptavidin to Au nanoclusters, a band is observed in the 1615 cm^{-1} shift region, corresponding to bands involved in C=N, C=C, and aromatic ring stretching modes. Although hints of other spectral features are apparent at this step, no other assignments could be made with confidence. Following brief exposure (0-1 minute) to Ag precipitating solution, the signal-to-noise ratio of the 1615 cm^{-1} peak is enhanced, and an additional broad peak at ~2100 cm^{-1} becomes apparent, likely corresponding to an additional mode of an aromatic ring moiety. Finally, following 5 minutes of exposure to Ag precipitating solution, several additional bands become apparent, including strong peaks at 1580 cm^{-1}, and 1100 cm^{-1}, as well as smaller peaks at ~1450 cm^{-1}, ~800 cm^{-1}, ~600 cm^{-1}, and ~400 cm^{-1}. Possible assignments for these peaks include, 1580 cm^{-1} and 1450 cm^{-1}: additional aromatic ring vibrations; 1100 cm^{-1}: C-S aromatic or C=S stretches; and 800 cm^{-1} and 600 cm^{-1}: alicyclic Cs or C-S stretches. Although plasmonic coupling from nanoparticles can result in altered selection rules of characteristic Raman modes, the band assignments show strong agreement with spectral signatures which would be expected from aromatic and heterocyclic side chains of amino acids in proteins. The large increase in spectral detail similarly encourages the prospect of this simple, single pot enhancement chemistry for calibrated single molecule detection of peptide toxins and DNA of interest. Possible indication of single molecule detection using the 5 minute enhanced sample was observed using a fast data collection mode, which is not averaged. In this mode, a single point spectrum is acquired and displayed at 2 second intervals. When solution data was collected in this manner, large temporal deviation was observed, with some spectra showing little or no features and others showing complex (2-5 peaks) data. Although without averaging, single features of this nature are usually attributed to cosmic spikes in the detector, more than 2 features could indicate diffusion of a single particle or aggregate through the detection volume, and a subsequent single molecule SERS readout. Finally, the presence of prominent spectral features known to be associated with modes of organo-sulfur compounds indicate that plasmonic coupling in this system may be directed from the Ag layer through the Au-maleimide-sulfur covalent couple.

2) Electrochemical Measurements

Mutagenesis Results

In Figure 10, Zhaohui Xu and his co-workers show the amino-acid sequence of GroEL[10]. Secondary structural elements are indicated by rectangles (a-helices) or arrows (b-strands) and extended strands. The a-helices are labeled A to R, and b-strands are numbered 1 to 19.

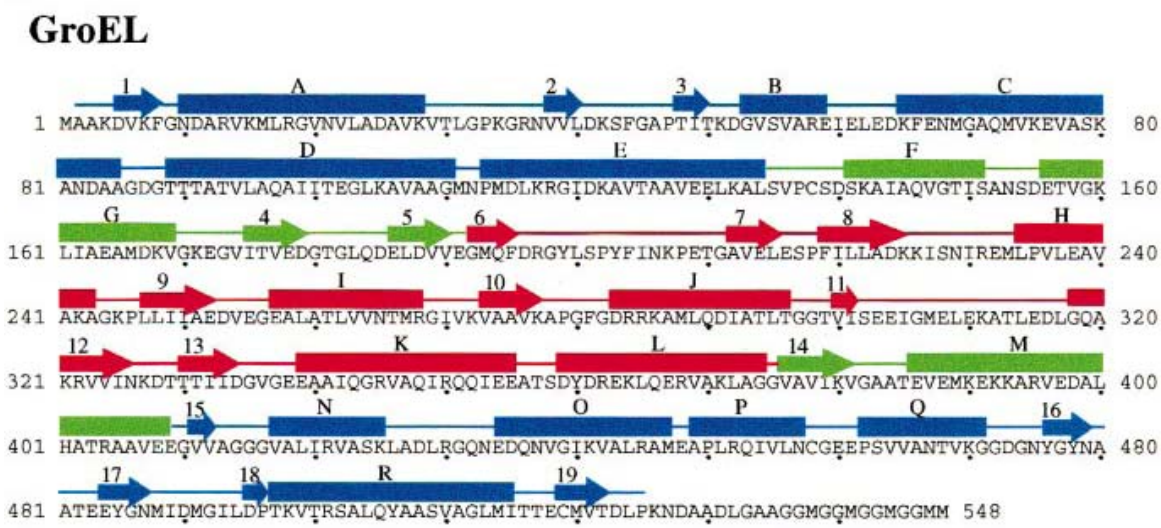

a

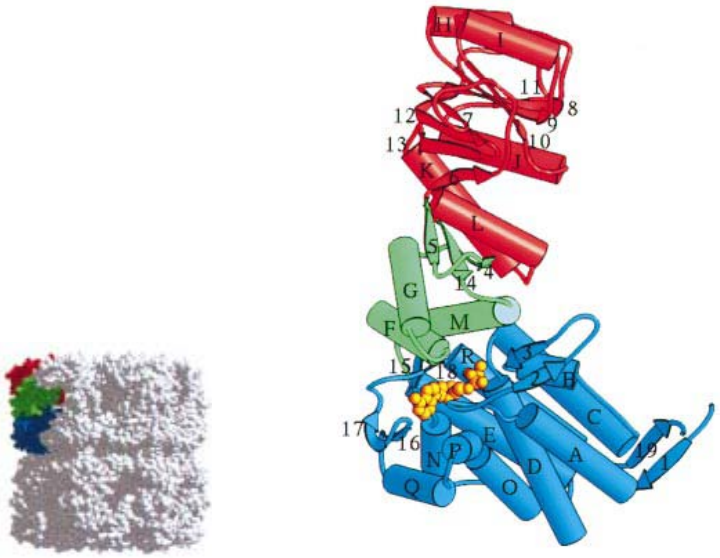

b **c**

Fig. 10: Amino acid sequence and tertiary structure of GroEL**.**

Color coding corresponds to the representations in b and c and denotes the domain in which the sequence segments occur; for GroEL, equatorial is blue, intermediate is green, apical is red. As illustrated above the Asp490 lies within the equatorial domain and replacing this amino acid with cysteine allowed for labeling with biotin maleimide, without compromising the proteins biological activity. Most importantly, this mutation did not inhibit binding of ATP and assisted folding of rhodanese.

Purification Results

The purification method was a combination of protocols described by Mendoza[12] and Quaite[17]. The yield of protein isolated from cultured *E.coli* was 28 mg total from 1L of culture. The western blot shown in Figure 11 displays four different fractions of GroEL collected after purification. The band running at about 60kDa after probing with GroEL Monoclonal Antibody (9A1/2), is the GroEL protein which is a 60kDa protein. The additional bands running below the 60kDa band are most likely due to nonspecific binding of the primary antibody utilized for detection of GroEL. In addition, the refolding of urea denatured rhodanese performed with our mutant GroEL proved that the purification treatment did not inhibit the biological activity of GroEL.

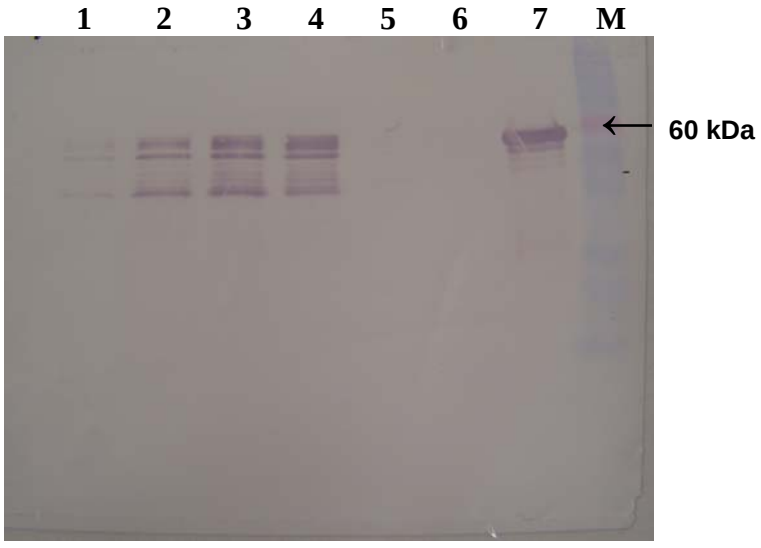

Fig. 11: Western blot of purified GroEL. Lanes 1 thru 4 display fractions collected after last purification step. Lane 7 displays commercial GroEL from Sigma-Aldrich.

Release of gold particles from immobilized chaperonins

Immobilization of the native GroEL via diazonium chemistry and the thiol gold protocol worked but required optimization (thus the cysteine substituted GroEL mutant). Table 1 shows the release of gold from immobilized GroEL. As higher concentrations of ATP were added, higher concentrations of Au particles were released. The AuNPs were incorporated into the GroEL chaperonin at the same concentration (2.78 µM GroEL) in each experiment and then ATP, at different concentrations, was added to release the gold. The gold was then detected in solution using an absorbance assay at 600 nm. The lower concentration looks like the control, showing no release, but at higher concentrations of ATP, release of gold occurs. The amount of ATP to release Au is a lot less in experiments conducted on unbound GroEL (Figure 12). This is explained by the fact that the protein is more rigid once immobilized so the concentration of ATP required for release will be higher.

ATP concentration	No ATP	20 µM ATP	200 µM ATP
Abs_{600}	0.009	0.008	0.019

Table 1: Absorbance assay showing release of Au particles upon addition of ATP

Release of gold particles from unbound chaperonins

Gold nanoparticles released into solution were detected electrochemically. The graph shows release of gold particles from chaperonin-gold complex for 2, 5, 10, 20, and 40 uM ATP addition (moving up the curve). The chaperonins and 2 nm

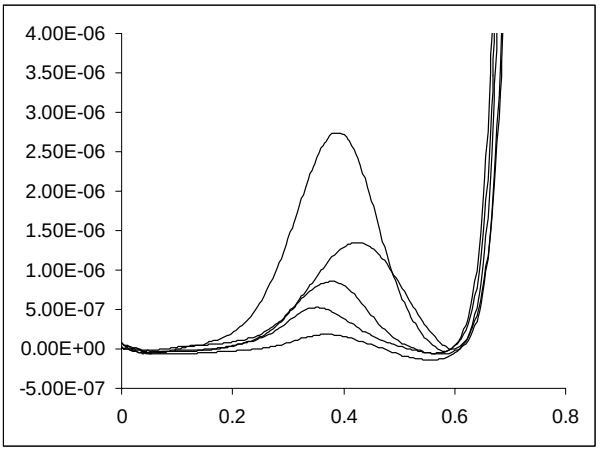

Fig. 12: Electrochemical detection of released gold nanoparticles.

Au nanoparticles were mixed for three days and then filtered through a 30000 cut-off centricon to remove unbound gold. For detection of ATP-released nanoparticles, different concentrations of ATP were added to equal aliquots of the solution containing the gold-protein complex. The solution was then filtered removing chaperonins and the released gold was dissolved in HBr/Br2 and analyzed using potentiometric stripping.

Discussion

Formation of complex nanomaterials would ideally involve single-pot reaction conditions with one reactive site per nanoparticle, resulting in a high yield of incrementally modified or oriented structures. Many studies in nanoparticle functionalization have sought to generate the highly uniform nanoparticles with tailorable surface chemistry necessary to produce such conjugates, with limited success. In order to overcome these limitations, we have modified commercially available nanoparticles with multiple potential reaction sites for conjugation with single ssDNAs, proteins, and small unilamellar vesicles. These approaches combined heterobifunctional and biochemical template chemistries with single molecule optical methods for improved control of nanomaterial functionalization.

Several interesting analytical results have been achieved by leveraging techniques unique to SNL, and provide multiple paths for future improvements for multiplex nanoparticle synthesis and characterization. Hyperspectral imaging has proven especially useful for assaying substrate immobilized fluorescent particles. Spectral images of CdSe nanoparticles at the single molecule level highlight the intrinsic emission variability from supposedly identical particles, allowing unambiguous monitoring of the effects of functionalization on a particle by particle basis. In dynamic environments, temporal correlation spectroscopies have been employed for tracking changes in diffusion/hydrodynamic radii, particle size distributions, and identifying mobile versus immobile sample fractions at unbounded dilution. Finally, Raman fingerprinting of biological conjugates has been enabled by resonant signal enhancement provided by intimate interactions with nanoparticles and composite nanoshells.

Multi-particle interactions between functionalized nanoparticles and mediated by biochemical recognition events provide a unique strategy amenable to both optical and electrochemical synthetic and detection schemes. In these studies, polymer stabilized, colloidal, and atomic cluster nanoparticles were employed, and found to have dramatically varying, environmentally dependent properties. Combined with the ubiquitous nano-biological structures; proteins, DNA, and phospholipid liposomes, enhanced materials tailoring and sensing have been achieved.

References

1. R.A. McMillan, *Nat. Mat*. 2, 214-215, 2003.
2. B. Burns, H. Ow, and U. Wiesner, *Chem. Soc. Rev*. 35,1028-1042, 2006.
3. P. Zhang, S. Rogelj, K. Nguyen, D. Wheeler, *JACS* 128 (38), 12410, 2006.
4. Grabarek, Z.and Gergely, J., *Anal. Biochem*. **185**, 131-135, 1990.
5. Mattson, G., *et al.,* A practical approach to cross-linking. *Molecular Biology Reports* **17:**167-183, 1993.
6. Hashida, S., *et al., J. Appl. Biochem.* **6,** 56-63, 1984.
7. M. B. Sinclair, D. M. Haaland, J. A. Timlin & H. D. T. Jones, *Applied Optics,* **45,** 3283-3291, 2006.
8. P. Hing and H. W. Muller, *Biophotonics,* 52-58, Sept. 2003.
9. Taguchi, H., Ueno, T., Tadakuma, H., Yoshida, M., Funatsu, T., *Nat. Biotechnol*., **19**: 861-865, 2001.
10. Xu, Z., Horwich, A.,Sigler,P., *Nature*, **388**: 741-750, 1997.
11. Kamireddi, M., Eisenstein, E., Reddy, P., *Protein Expression and Purification*, **11**:47-52, 1997.
12. Mendoza, J.A., Rogers, E., Lorimer, G. H., and Horowitz, P.M., *J. Biol. Chem.*, **266**:13044-13049, 1991.
13. Sorbo, B. H. *Acta Chem. Scand.*, **7**: 1129-1136, 1953.
14. Battacharjee, C-.H. Hsu, C-.H. Lu, W.H. Chang, *Physica E.*, 33, 388-393, 2006.
15. N.A. Kotov "Nanoparticle assemblies and superstructures", CRC Press. Boca Raton, 2006.
16. Nie, S.; Emory, S. R., *Science*, 275, (5303), 1102-1106, 1997.
17. Quaite-Randall, E., Joachimiak, A., *Methods and Molecular Biology*, ***140***: 29-39, 2000.

Distribution List

2	MS0892	Susan Brozik	Org. 1714
1	MS0899	Technical Library	9536 (electronic copy)
1	MS0123	D. Chavez, LDRD Office	1011


Sandia National Laboratories